analytical chemistry

Technical Note

pubs.acs.org/ac

Nanopipette-Based Electroplated Nanoelectrodes

Rui Hao and Bo Zhang*

Department of Chemistry, University of Washington, Seattle, Washington 98195, United States

ABSTRACT: Here, we report a nanopipette-based electrochemical approach to prepare metal nanoelectrodes with excellent control over electrode size, shape, and thickness of the insulation wall. Nanoelectrodes are prepared by electrochemical plating in a laser-pulled quartz nanopipette tip immersed in a liquid gallium/indium alloy electrode, which not only protects the ultrasmall quartz tip but also starts electrodeposition from the tip orifice. This versatile approach enables reproducible fabrication of electrodes of several different metals, including gold, platinum, silver, and copper. Moreover, nanoelectrodes with varying sizes can be easily prepared by focused ion-beam milling. A unique aspect of this method is the control over the thickness of quartz insulation walls relative to the size of the electroactive surface enabling control of the RG (defined as the radius of the insulating sheath over the radius of the active metal electrode). As such, these nanoelectrodes may be especially attractive as useful nanoprobes in high-resolution imaging applications, such as scanning electrochemical microscopy.

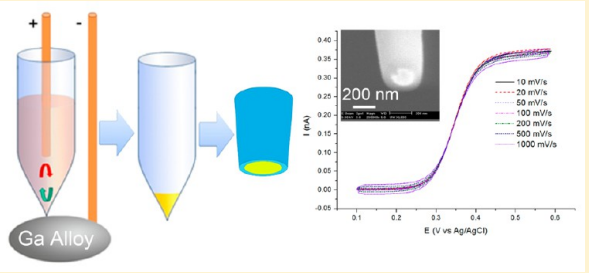

Electrodes of nanometer dimensions or nanoelectrodes are tools of key importance in nanoelectrochemistry research. Nanoelectrodes, usually defined as electrodes with a critical dimension in the 1−100 nm range, have found useful application in numerous studies, including high-resolution imaging with scanning electrochemical microscopy (SECM),[1−5] immobilization and further study of single molecules and nanoparticles,[6−14] chemical sensing from inside and outside of single cells,[15−18] and fundamental understanding of electron-transfer kinetics and double layer effects.[19−21]

A major challenge in nanoelectrochemistry research has been the irreproducible production of nanoelectrodes with controlled size, shape, and functionality. This is largely due to their nanoscale dimensions and the somewhat unavoidable involvement of human handling with benchtop equipment. Physical thinning and chemical etching of a conductive microwire followed by polymer insulation is a popular method to reduce active electrode size down to the nanometer scale.[22−30] Conversely, pyrolysis of hydrocarbons and interfacial reactions could deposit electrode materials (carbon or metal) in insulating glass nanopipettes to fabricate nanoelectrodes.[31−37] Electrode geometry is determined by glass nanopipettes. Because of their small size and excellent electrochemical properties, carbon nanotubes are also used to prepare nanoelectrodes.[38−45] Laser pulling of glass-sealed metal wires is widely used for nanoelectrode fabrication,[46−50] allowing fabrication of glass or quartz-insulated platinum or gold disk nanoelectrodes from 1 to >100 nm in radii.[19] However, laser-pulled nanoelectrodes bear thick glass insulation walls with thicknesses often >10 times greater than the radius of the electroactive area. Other methods often yield conical nanoelectrodes with somewhat random size, shape, and poor reproducibility.

The use of nanoelectrodes for high-resolution electrochemical imaging applications, such as SECM, requires small nanoelectrodes with controlled size and shape. RG ratio, which is defined as the ratio between the radius of the insulating sheath and that of the active electrode area, is a key geometric factor in electrochemical imaging and nanoscale electrochemistry in general.[51,52] Nanoelectrode probes with small RGs can minimize blockage of diffusion from an insulating sheath and allow extremely small tip-to-substrate separation, which would result in greater sensitivity.[52] Typical methods for small RG ultramicroelectrode probes include polishing or etching to shrink down the existing insulation,[47,53,54] the use of a thin polymer coating,[25,55−58] and chemical deposition in templates.[33,35,37] However, many of the reported methods are only useful for microelectrode probes, and a general method for fabricating nanoelectrodes with controlled size, shape, and RG ratio has yet to be determined.

In this work, we report a general method for the fabrication of metal nanoelectrodes with small and controllable RG ratio and size and a wide selection of electrode materials. A key aspect of this method is the use of a quartz nanopipette as a unique template to electrodeposit metal inside the pipet walls. Nanometer-sized quartz pipet tips are protected by immersing into a liquid eutectic gallium−indium alloy (EGaIn) electrode and electroplating from inside the pipettes. Several metals, including gold, platinum, silver, and copper, have been used for nanoelectrode fabrication. The RG ratio of the nanoelectrodes is predetermined by the ratio of the outside/inside diameters of the quartz tubing, which can be fine-tuned by a simple laser heating procedure prior to laser pulling, and focused ion-beam

Received: September 18, 2015
Accepted: November 28, 2015
Published: November 28, 2015

DOI: 10.1021/acs.analchem.5b03548
Anal. Chem. 2016, 88, 614−620

(FIB) milling was employed to expose the nanoelectrodes for size control. The use of theta quartz tubing allows for the preparation of dual nanoelectrodes and a single nanoelectrode attached to a quartz nanopipette. Nanoelectrodes were fully characterized with steady-state voltammetry, scanning electron microscopy (SEM), and transmission electron microscopy (TEM). Future applications of such nanoelectrodes include high-resolution electrochemical imaging with SECM and single-nanoparticle electrocatalysis.

EXPERIMENTAL SECTION

Chemicals and Materials. Eutectic gallium−indium alloy (EGaIn, Alfa Aesar), chloroauric acid ($HAuCl_4$, Aldrich), chloroplatinic acid (H_2PtCl_6, Aldrich), silver trifluoroacetate (CF_3COOAg, Alfa Aesar), copper sulfate ($CuSO_4$, Mallinckrodt Baker), boric acid (H_3BO_3, Mallinckrodt Baker), pyrrole (Py, Aldrich), *p*-aminothiophenol (PATP, Aldrich), ferrocene (Fc, Fluka), ferrocene methanol (FcMeOH, Aldrich), potassium ferricyanide ($K_3Fe(CN)_6$, Aldrich), lithium perchlorate ($LiClO_4$, Aldrich), tetra-*n*-butylammonium hexafluorophosphate ($TBAPF_6$, Aldrich), potassium nitrate (KNO_3, Aldrich), sodium hydroxide (NaOH, Aldrich), isopropanol (IPA, Fluka), butanol (Fluka), hydrochloride acid (HCl, Fluka), and acetonitrile (ACN, Fluka) were of reagent grade quality or better and used without further purification. Silver wire (99.9%, 0.127 mm diameter) was purchased from Alfa Aesar. Single barrel quartz tubing with filament (0.7 mm I.D./1.0 mm O.D. and 0.5 mm I.D./1.0 mm O.D.) and theta quartz tubing (0.9 mm I.D./1.2 mm O.D./0.15 mm septum) were purchased from Sutter Instrument. Colloidal graphite (isopropanol base) was purchased from EB Science.

Instruments. A laser pipet puller (P-2000, Sutter Instrument) was used for the preparation of quartz nanopipettes. A DC power supply (1610 BK Precision) was used to deposit the metal or polymerized pyrrole in the nanopipettes. A ChemClamp voltammeter/amperometer (Dagan) was employed as a potentiostat in all voltammetry testing. The potentiostat was interfaced to a Dell computer through a PCI-6521 board (National Instrument) via a BNC-2090 breakout accessory (National Instrument). Voltammetric data were recorded using in-house virtual instrumentation written in LabView 8.6 (National Instrument). A one-compartment, two-electrode cell was used with the cell and preamplifier placed in a home-built Faraday cage. A homemade Ag/AgCl electrode was used as the reference/counter electrode. TEM images were acquired on an FEI Tecnai G^2 F20 microscope. SEM imaging and FIB milling were performed on an FEI XL830 Dual Beam system.

Quartz Nanopipettes. Quartz nanopipettes were prepared by pulling a piece of quartz tubing on a P-2000 laser puller. Sample pulling programs are listed as follows. For a 0.7 mm I.D./1.0 mm O.D. capillary, a good pulling program is heat = 610, filament = 4, velocity = 90, delay = 140, and pull = 255. For a 0.5 mm I.D./1.0 mm O.D. capillary, a good pulling program is heat = 600, filament = 3, velocity = 90, delay = 140, and pull = 255. For a 0.9 mm I.D./1.2 mm O.D. capillary with 0.15 mm septum, a good program can be heat = 700, filament = 4, velocity = 60, delay = 140, and pull = 150.

To increase the glass wall thickness and change the I.D./O.D. ratio of the pulled nanopipette, we fixed the pulling arms by an aluminum clamp after a capillary was mounted on the puller and an additional heating cycle was applied. To obtain a nanopipette with "RG" = 3, we used the following program on a piece of quartz tubing (I.D. 0.5 mm/O.D. 1.0 mm): heat = 750, filament = 2, velocity = 90, delay = 200, and heating time = 30 s for 2 times with a 30 s interval. The heat value can be adjusted accordingly to pull quartz pipettes with different "RGs".

Metal Deposition. For gold deposition, a pulled nanopipette was filled with an isopropanol solution of 25 mg/mL (~70 mM) chloroauric acid and 0.1 M $LiCO_4$. A thin Ag/AgCl electrode was inserted into the solution in the pipettes. Then, the nanopipette was carefully inserted into a liquid EGaIn electrode, and a voltage of 0 V was applied between alloy electrodes and the Ag/AgCl electrode. After 2 h, the nanopipette was taken out of the EGain electrode and rinsed from the inside by acetonitrile and dried. The remaining alloy residue on the glass walls was removed by rinsing in a 1 M HCl solution. The nanoelectrode was milled with FIB to expose the gold disk. Electrodes of other metals can be prepared using the following deposition conditions: for Pt, an IPA solution of 10 mg/mL of chloroplatinic acid and 0.1 M $LiCO_4$ was used with a −300 mV deposition voltage; for Ag, an IPA solution of 10 mg/mL of silver trifluoroacetate and 0.1 M $LiCO_4$ was used with a −300 mV voltage; and for Cu, an aqueous solution of 0.2 M $CuSO_4$ and 0.1 M boric acid was used with a −800 mV voltage.

Electropolymerization of Polypyrrole. The nanopipette was further filled with a conductive polymer polypyrrole to facilitate making an electric contact to the metal wire. To do so, the electrode-containing nanopipette was filled with an acetonitrile solution containing 2 M pyrrole and 0.5 M $LiClO_4$, dipped into a conductive solution of colloidal graphite, and dried. Then, the nanopipettes were carefully dipped into the alloy liquid metal, and a thin Ag/AgCl electrode was again used inside the pipet to electropolymerize pyrrole onto the metal electrode. A DC voltage of +1.5 V was applied on the electroplated metal for 12 h after which the nanopipette was further rinsed from inside by acetonitrile, and the remaining metal alloy was cleaned by 10% HCl, water, and IPA. A piece of 10 μm diameter tungsten wire was used to make direct contact to the polypyrrole/nanoelectrode assembly.

RESULTS AND DISCUSSION

Depending on the pulling conditions and the glass/quartz tubing, a laser-pulled nanopipette can be prepared to have a tip diameter of 10−100 nm with sidewalls as thin as a few nanometers.[59] Therefore, it is generally very challenging to deposit guest materials in the nanopipettes in an electrochemical setup due to the difficulty of making a leakage-free electric contact to the pipet tip. Shao and co-workers have reported a method to chemically deposit gold in the pipet tip by placing a water-soluble gold salt in the pipet and immersing the tip in an organic solvent containing decamethylferrocene as a reducing agent. The establishment of a liquid/liquid interface was believed to be the key to obtain metal growth in the pipet tip. Baker and co-workers have reported deposition of parylene onto a quartz nanopipette/nanorod and conversion of parylene to conductive carbon for carbon nanoelectrodes with another layer of parylene as an insulating sheath.[31] Unwin and co-workers reported a facile method of pyrolytic carbon deposition from butane in a quartz pipet.[35] Mirkin and co-workers demonstrated fabrication of a carbon-filled quartz pipet from chemical vapor deposition with methane as the precursor.[14]

Here, we thought of using liquid metals as the electrode materials to avoid breakage of the small pipet tip and to establish a leak-free electric contact for electroplating. Because

DOI: 10.1021/acs.analchem.5b03548
Anal. Chem. 2016, 88, 614−620

mercury is toxic and can easily dissolve lots of metals, including gold, EGaIn with a melting point of 15.7 °C can be considered as a useful electrode material for this experiment. Extra care is needed when inserting a nanopipette into the alloy because the surface tension of EGaIn is ~624 mN/m,[60] which is much greater than that of mercury (476 mN/m) and water (72.75 mN/m). Moreover, the surface oxide layer of the alloy should also be removed prior to pipet insertion. Isopropanol was selected as the solvent for the deposition because it fills the nanopipette more rapidly than water without trapping air bubbles in the tip.

Electroplating of gold inside a quartz nanopipette takes two separate stages: a chemical reduction stage upon contact of chloroauric acid and EGaIn and a subsequent electrochemical reduction and further growth of gold. Chloroauric acid would be immediately reduced to gold upon contact with the EGaIn alloy considering that the standard potentials of $AuCl_4^-$/Au, Ga^{3+}/Ga, and In^{3+}/In are +0.93, −0.53, and −0.34 V, respectively, relative to NHE. This would create a thin layer of gold metal isolating the close contact of the chloroauric acid with the EGaIn alloy. Further growth of gold is driven by applying a 0 V voltage on the thin gold film relative to a Ag/AgCl electrode. The standard potential of Ag/AgCl is +0.22 V relative to NHE, so even though 0 V was applied, the deposition of gold would still proceed on the gold electrode. The use of 0 V is only an optimized condition for growing gold nanostructures with good quality.

Scheme 1. (a) Electrodeposition of Metal in a Nanopipette, (b) Electropolymerization of PPy for Making Direct Electric Contact to the Electrode, and (c) FIB Milling

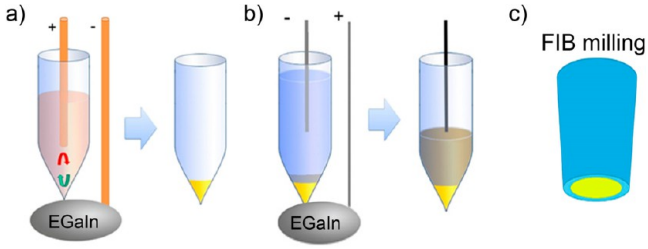

In this template-based approach, the shape and size of the gold nanoelectrode depend heavily on the quartz nanopipette. Hence, for the purpose of making nanoelectrodes with controlled size and RG ratio, quartz nanopipettes with controlled size and "RG" ratio are needed (considering the hollow space as electrode). For a laser-pulled nanoelectrode, RG is almost always above 10 and can sometimes approach 40.[49] Although polishing or HF etching can decrease the RG, this would be time-consuming and extremely challenging for electrodes below 100 nm.[61]

Our approach enables easy and reproducible control over electrode RG by choosing and adjusting quartz tubing with a desired "RG" ratio prior to pipet pulling. To obtain RG = 1.42 or 2 electrode, quartz tubing of 0.7 I.D./1.0 O.D. or 0.5 I.D./1.0 O.D. can be directly selected from commercial sources. However, it is hard to pull quartz nanopipettes of the larger "RGs" due to a limited selection of commercially available quartz tubing. Therefore, we used a simple laser heating procedure to tune the "RG" of the pulled nanopipettes. Laser heating without pull causes both the I.D. and O.D. of quartz tubing to decrease. However, the bore changes faster than the external diameter and, eventually, the bore of the tubing will completely close with continuous heating. This enables us to fine tune the I/O ratio of the quartz tubing and obtain nanopipettes with controlled "RGs", which are further used for metal deposition. Figure 1 displays four quartz nanopipettes

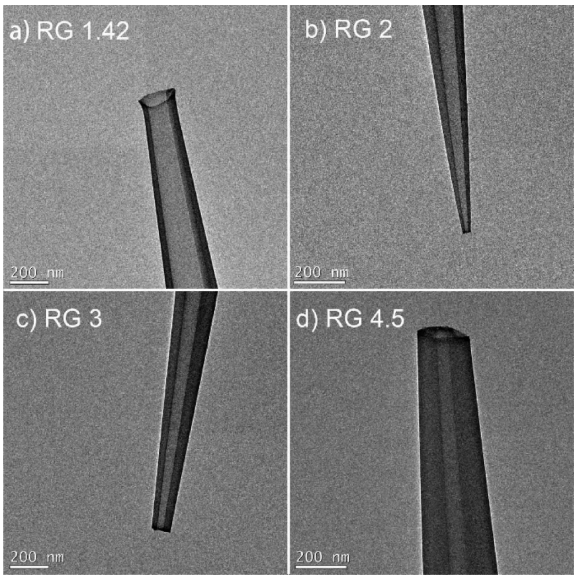

Figure 1. Pulled quartz nanopipettes with four different RGs: (a) 1.42, (b) 2, (c) 3, and (d) 4.5.

with different RGs: (a) 1.42, (b) 2, (c) 3, and (d) 4.5. Nanopipittes with larger RGs can still be obtained with this technique, but they are less useful than smaller ones for future imaging experiments. It is worth noting that the sheath could be thinner than 50 nm for small RG nanoelectrodes; hence, the tubing materials should be quartz but not borosilicate glass, which could be conductive under some extreme conditions.[62]

FIB milling was employed to shorten the metal-filled nanopipette and expose a fresh metal nanoelectrode. Gold nanoelectrodes with radii ranging from 20 to 500 nm can be reproducibly obtained with this method. Figure 2 exhibits SEM images (52 degree sample) of the cross-section of gold nanoelectrodes with electrode radii of 350, 200, 170, 125, 67, and 30 nm. Some of the quartz walls are slightly thicker, but the average RG for these electrodes is ~1.4. The metal surfaces are flat, and no pinholes can be observed at this magnification. The dark round spots on the inside of the quartz walls are from the quartz filaments, which help facilitate solution filling prior to electroplating. It is worth noticing that even the sharp corners near the filaments in Figures 2a–d were fully occupied by gold, indicating smooth and complete electrochemical growth. There are several key parameters that limit our ability to examine the finely detailed structures of the milled metal surfaces under 100 nm. These include the insulating nature of the quartz walls, a strong charging effect, the vibration of the tips during SEM imaging, and the limited spatial resolution of the SEM itself. A thin carbon coating was selected to help examine the quality of the metal deposition in smaller pipettes. A similar cross-section view can be obtained in the 50 nm nanoelectrode with a smooth and pinhole-free metal surface.

TEM images of gold nanoelectrodes with RGs of 1.4, 2, and 3 are shown in Figure 3a, e, and f. All three images depict solid and continuous gold deposition in the nanopipette template. Figure 3d shows a high-resolution TEM (HRTEM) image of a selected tip area of a gold nanoelectrode with an RG of 1.4. The

DOI: 10.1021/acs.analchem.5b03548
Anal. Chem. 2016, 88, 614−620

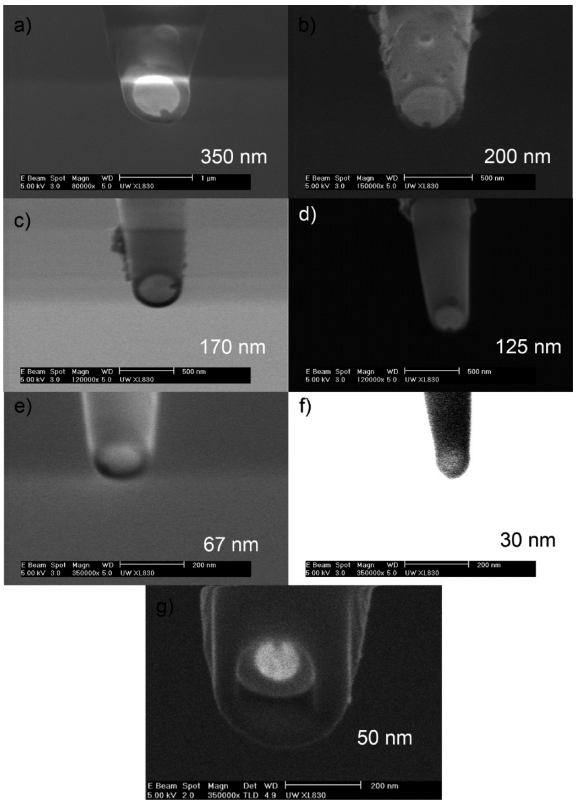

Figure 2. Carbon-coated gold nanoelectrodes with radii of (a) 350, (b) 200, (c) 170, (d) 125, (e) 67, (f) 30, and (g) 50 nm.

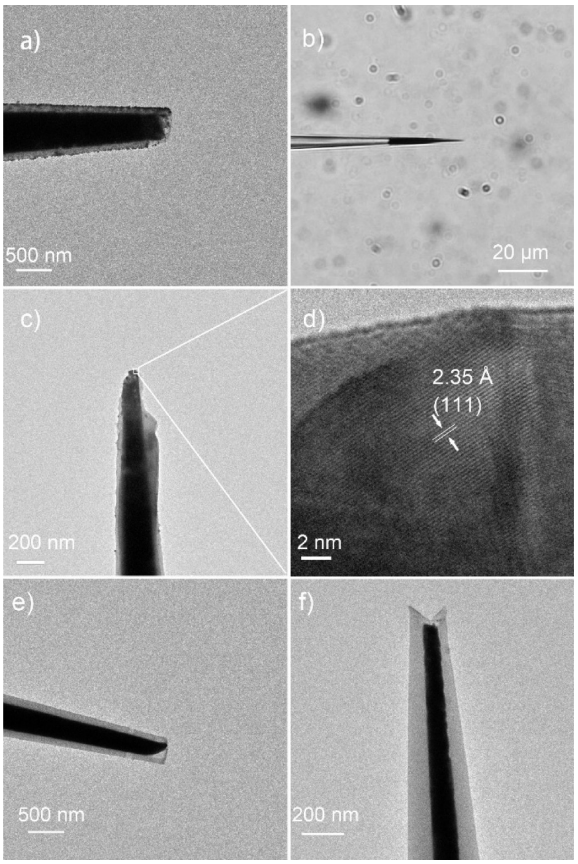

Figure 3. (a) TEM and (b) optical images of an RG 1.4 gold nanoelectrode; (c) TEM and (d) HRTEM images of another RG 1.4 gold nanoelectrode, and TEM images of (e) RG 2 and (f) RG 3 gold nanoelectrodes.

average RG of the electrodes from an O.D./I.D. = 1.43 quartz tubing was 1.43 ± 0.08. The clear lattice fringes with 0.235 nm spacing indicate (111) plane of face-centered cubic gold (JCPDS 04-0784). After electrochemical growth for 2 h, the length of the gold in the nanopipette was around 50 μm according to the optical image in Figure 3b. The success rate of the electroplating process was approximately 70%. Extra deposition time would not always result in longer gold deposition, which could be due to slow growth, and the growth can sometimes be easily interrupted. In most cases, however, it is difficult to contact the gold inner surface by thin wires. Therefore, further growth of the conductive portion from inside the nanopipette is necessary. Polypyrrole (PPy) was selected to further deposit onto the inner gold surface because the growth rate of polypyrrole is much higher than that of gold (9 atoms/electron for PPy, 1/3 atoms/electron for gold). Lithium perchlorate[63] was used as the electrolyte in electrochemical polymerization and dopant in the PPy. The length of the PPy structure could reach up to several millimeters after 12 h of deposition.

Steady-state voltammetry was used to evaluate the electrochemical performance of nanopipette-based gold nanoelectrodes. Considering a disk-shaped nanoelectrode with thin insulation walls, the diffusion-limited steady-state current can be estimated using the equation

$$i_d = XnFDC_b r \quad (1)$$

where n is the number of electrons transferred per redox molecule, F is the Faraday's constant, r is the electrode radius, and D and C_b are the diffusion coefficient and bulk concentration of the redox molecule, respectively. The geometric factor X is 4 for electrodes with RG ≫ 10 or with infinitely large insulation walls. For electrodes with small RGs, the factor can be determined by the equation[64]

$$X = 4 + 4b(R_g - c)^d \quad (2)$$

where b, c, and d are 0.138, 0.6723, and 0.8686 respectively. On the basis of this equation, X should be 4.7 for RG = 1.4 and 4.43 for RG = 2 electrodes. We characterized the steady-state voltammetry of two nanoelectrodes with RG 1.4 and 2.0 at scan rates from 10 to 1000 mV/s in ferrocene, and the results are shown in Figure 4. Both electrodes exhibit well-defined sigmoidal CVs with little hysteresis between the forward and backward scans even at 1 V/s. The limiting currents in Figure 4 are measured at 0.38 nA (Figure 4a) and 0.24 nA (Figure 4b), which according to eq 1 correspond to electrode radii of 70 and 45 nm, respectively. These results closely match the SEM results shown in the insets of Figure 4.

By using theta barrel quartz tubing, one can prepare dual nanoelectrodes or a single nanoelectrode with an attached open nanopipette for possible delivery of solution species, such as a stimulation species for neurochemical sensing. Figure 5a shows a pulled quartz theta nanopipette with both sides filled by gold, and Figure 5b shows another theta pipet with only one side filled by gold. Both samples were coated with carbon prior to SEM imaging for better imaging quality. Similar to the single barrel nanopipettes, these nanopipettes were fully filled by gold metal and exhibited smooth and pinhole-free surfaces even at the sharp corners. As shown in Figure 5c, the TEM image of the gold dual nanoelectrode exhibited a clear septum and no

DOI: 10.1021/acs.analchem.5b03548
Anal. Chem. 2016, 88, 614−620

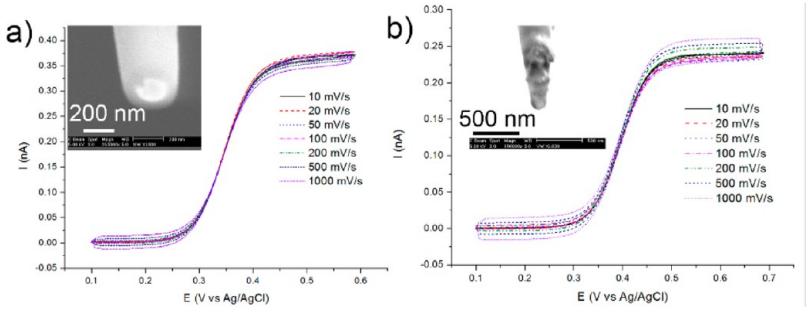

Figure 4. Steady-state CV responses of (a) RG 2 and (b) RG 1.42 gold nanoelectrodes in 5 mM ferrocene/0.2 M $TBAPF_6$ ACN solution with varying scan rates and corresponding SEM images (insert).

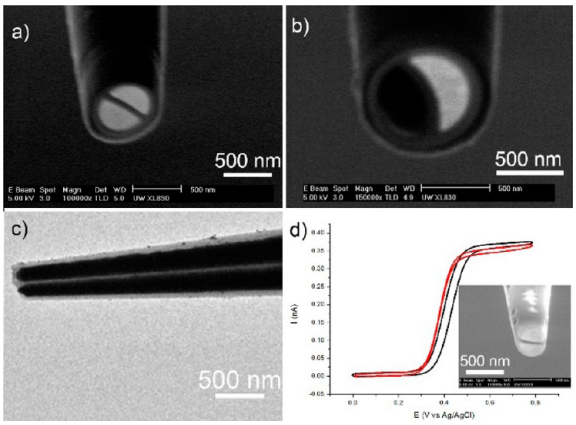

Figure 5. (a) SEM image of a dual nanoelectrode, (b) SEM image a single nanoelectrode with an attached nanopipette, (c) TEM image of a gold dual nanoelectrode, and (d) steady-state CVs at 50 mV/s of a dual nanoelectrode in 5 mM ferrocene/0.2 M $TBAPF_6$ ACN solution and corresponding SEM image (insert).

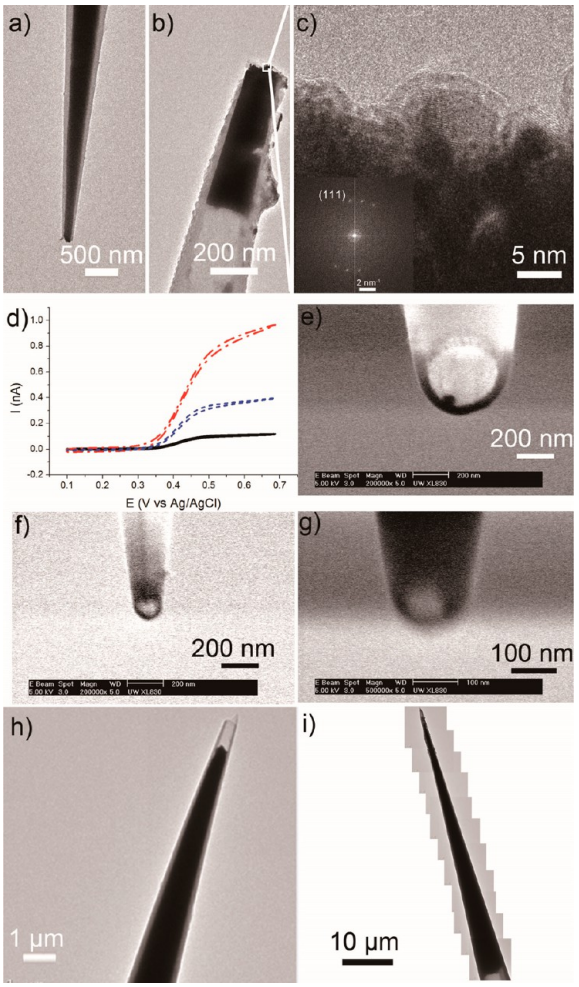

Figure 6. (a) TEM images of a Pt nanoelectrode; (b) TEM and (c) HRTEM image of another Pt nanoelectrode, the inset of which is the FFT result of the HRTEM image; (d) steady-state CVs at 50 mV/s of three Pt nanoelectrodes in 5 mM ferrocene/0.2 M $TBAPF_6$ ACN solution with their corresponding SEM images shown in (e) (red), (f) (blue), and (g) (black); (h) TEM image of a copper nanoelectrode; and (i) composite TEM image of a silver nanoelectrode.

apparent void space, indicating good deposition quality. A dual nanoelectrode was further characterized by cyclic voltammetry in 5 mM ferrocene, and the results are shown in Figure 5d along with its corresponding SEM image. The CV response of the dual nanoelectrode was obtained by measuring each electrode separately. The CVs are found to be similar in magnitude but independent of each other, indicating good performance.

Our approach can also be used to prepare nanoelectrodes of other metals. Panels a and b in Figure 6 show TEM images of a 50 nm and a 100 Pt nanoelectrode, respectively. Figure 6c is an HRTEM image of the Pt nanoelectrode in Figure 6b. The FFT of the HRTEM image shows three pairs of dots, which can be assigned to the (111) facet of platinum (JCPDS 04-0802). Figure 6d shows steady-state CVs in 5 mM ferrocene of three Pt nanoelectrodes of which the SEM images are shown in Figures 6e–g. Besides platinum and gold, silver and copper nanoelectrodes (Figure 6h and i, respectively) can also be prepared.

■ CONCLUSIONS

We have demonstrated a useful method to prepare metal nanoelectrodes with controllable size, shape, and RG using laser-pulled quartz nanopipettes as template. This method involves the preparation of a quartz nanopipette template using laser pulling, fine-tuning its "RG" ratio, and subsequent electrochemical deposition of metal inside the pipet template using EGaIn as a liquid electrode. FIB milling allows clean electrode cutting and metal exposure. Compared with previous nanoelectrode fabrication strategies, this method has several advantages including easy manipulation and control over the size and RG of the nanoelectrode, a wide selection of the electrode materials by using different metal precursors, and preparation of multibarrel electrodes with control over electrode/pipet configuration. Nanoelectrodes prepared

DOI: 10.1021/acs.analchem.5b03548
Anal. Chem. 2016, 88, 614–620

through this approach are disk-shape and have ultrathin quartz walls flush with the electroactive material. These features may facilitate their future use in ultrahigh resolution electrochemical imaging with SECM.

AUTHOR INFORMATION

Corresponding Author

*E-mail: zhang@chem.washington.edu. Tel: 206-543-1767. Fax: 206-685-8665.

Notes

The authors declare no competing financial interest.

ACKNOWLEDGMENTS

The authors gratefully acknowledge financial support from the AFOSR MURI (FA9550-14-1-0003). Part of this work was conducted at the University of Washington NanoTech User Facility, a member of the National Science Foundation, National Nanotechnology Infrastructure Network (NNIN).

REFERENCES

(1) Mirkin, M. V.; Fan, F. R. F.; Bard, A. J. *J. Electroanal. Chem.* **1992**, *328*, 47−62.
(2) Velmurugan, J.; Sun, P.; Mirkin, M. V. *J. Phys. Chem. C* **2009**, *113*, 459−464.
(3) Sun, T.; Yu, Y.; Zacher, B. J.; Mirkin, M. V. *Angew. Chem., Int. Ed.* **2014**, *53*, 14120−14123.
(4) Kim, J.; Kim, B.-K.; Cho, S. K.; Bard, A. J. *J. Am. Chem. Soc.* **2014**, *136*, 8173−8176.
(5) Kranz, C. *Analyst* **2014**, *139*, 336−352.
(6) Fan, F. R. F.; Kwak, J.; Bard, A. J. *J. Am. Chem. Soc.* **1996**, *118*, 9669−9675.
(7) Boldt, F. M.; Heinze, J.; Diez, M.; Petersen, J.; Borsch, M. *Anal. Chem.* **2004**, *76*, 3473−3481.
(8) Xiao, X.; Bard, A. J. *J. Am. Chem. Soc.* **2007**, *129*, 9610−9612.
(9) Fan, F. R. F.; Bard, A. J. *Science* **1997**, *277*, 1791−1793.
(10) Xiao, X.; Fan, F.-R. F.; Zhou, J.; Bard, A. J. *J. Am. Chem. Soc.* **2008**, *130*, 16669−16677.
(11) Murray, R. W. *Chem. Rev.* **2008**, *108*, 2688−2720.
(12) Shan, X.; Díez-Pérez, I.; Wang, L.; Wiktor, P.; Gu, Y.; Zhang, L.; Wang, W.; Lu, J.; Wang, S.; Gong, Q.; Li, J.; Tao, N. *Nat. Nanotechnol.* **2012**, *7*, 668−672.
(13) Li, Y.; Cox, J. T.; Zhang, B. *J. Am. Chem. Soc.* **2010**, *132*, 3047−3054.
(14) Yu, Y.; Gao, Y.; Hu, K. K.; Blanchard, P. Y.; Noel, J. M.; Nareshkumar, T.; Phani, K. L.; Friedman, G.; Gogotsi, Y.; Mirkin, M. V. *ChemElectroChem* **2015**, *2*, 58−63.
(15) Sun, P.; Laforge, F. O.; Abeyweera, T. P.; Rotenberg, S. A.; Carpino, J.; Mirkin, M. V. *Proc. Natl. Acad. Sci. U. S. A.* **2008**, *105*, 443−448.
(16) Li, Y.-T.; Zhang, S.-H.; Wang, L.; Xiao, R.-R.; Liu, W.; Zhang, X.-W.; Zhou, Z.; Amatore, C.; Huang, W.-H. *Angew. Chem., Int. Ed.* **2014**, *53*, 12456−12460.
(17) Rees, H. R.; Anderson, S. E.; Privman, E.; Bau, H. H.; Venton, B. J. *Anal. Chem.* **2015**, *87*, 3849−3855.
(18) Liu, Y.; Li, M.; Zhang, F.; Zhu, A.; Shi, G. *Anal. Chem.* **2015**, *87*, 5531−5538.
(19) Oja, S. M.; Wood, M.; Zhang, B. *Anal. Chem.* **2012**, *85*, 473−486.
(20) Sun, P.; Mirkin, M. V. *Anal. Chem.* **2006**, *78*, 6526−6534.
(21) Dickinson, E. J. F.; Compton, R. G. *J. Electroanal. Chem.* **2011**, *661*, 198−212.
(22) Noel, J.-M.; Velmurugan, J.; Gokmese, E.; Mirkin, M. V. *J. Solid State Electrochem.* **2013**, *17*, 385−389.
(23) Lee, S.-K.; Yoon, Y.-H.; Kang, H. *Electrochem. Commun.* **2009**, *11*, 676−679.
(24) Woo, D. H.; Kang, H.; Park, S. M. *Anal. Chem.* **2003**, *75*, 6732−6736.
(25) Slevin, C. J.; Gray, N. J.; Macpherson, J. V.; Webb, M. A.; Unwin, P. R. *Electrochem. Commun.* **1999**, *1*, 282−288.
(26) Baker, W. S.; Crooks, R. M. *J. Phys. Chem. B* **1998**, *102*, 10041−10046.
(27) Chen, S. L.; Kucernak, A. *Electrochem. Commun.* **2002**, *4*, 80−85.
(28) Chen, S. L.; Kucernak, A. *J. Phys. Chem. B* **2002**, *106*, 9396−9404.
(29) Huang, W. H.; Pang, D. W.; Tong, H.; Wang, Z. L.; Cheng, J. K. *Anal. Chem.* **2001**, *73*, 1048−1052.
(30) Abbou, J.; Demaille, C.; Druet, M.; Moiroux, J. *Anal. Chem.* **2002**, *74*, 6355−6363.
(31) Thakar, R.; Weber, A. E.; Morris, C. A.; Baker, L. A. *Analyst* **2013**, *138*, 5973−5982.
(32) McNally, M.; Wong, D. K. Y. *Anal. Chem.* **2001**, *73*, 4793−4800.
(33) Yu, Y.; Noel, J. M.; Mirkin, M. V.; Gao, Y.; Mashtalir, O.; Friedman, G.; Gogotsi, Y. *Anal. Chem.* **2014**, *86*, 3365−3372.
(34) McKelvey, K.; Nadappuram, B. P.; Actis, P.; Takahashi, Y.; Korchev, Y. E.; Matsue, T.; Robinson, C.; Unwin, P. R. *Anal. Chem.* **2013**, *85*, 7519−7526.
(35) Takahashi, Y.; Shevchuk, A. I.; Novak, P.; Zhang, Y.; Ebejer, N.; Macpherson, J. V.; Unwin, P. R.; Pollard, A. J.; Roy, D.; Clifford, C. A.; Shiku, H.; Matsue, T.; Klenerman, D.; Korchev, Y. E. *Angew. Chem., Int. Ed.* **2011**, *50*, 9638−9642.
(36) Sun, P.; Zhang, Z. Q.; Guo, J. D.; Shao, Y. H. *Anal. Chem.* **2001**, *73*, 5346−5351.
(37) Zhu, X.; Qiao, Y.; Zhang, X.; Zhang, S.; Yin, X.; Gu, J.; Chen, Y.; Zhu, Z.; Li, M.; Shao, Y. *Anal. Chem.* **2014**, *86*, 7001−7008.
(38) Lai, S. C. S.; Dudin, P. V.; Macpherson, J. V.; Unwin, P. R. *J. Am. Chem. Soc.* **2011**, *133*, 10744−10747.
(39) Patil, A. V.; Beker, A. F.; Wiertz, F. G. M.; Heering, H. A.; Coslovich, G.; Vlijm, R.; Oosterkamp, T. H. *Nanoscale* **2010**, *2*, 734−738.
(40) Gong, K.; Chakrabarti, S.; Dai, L. *Angew. Chem., Int. Ed.* **2008**, *47*, 5446−5450.
(41) Zhang, M.; Liu, K.; Xiang, L.; Lin, Y.; Su, L.; Mao, L. *Anal. Chem.* **2007**, *79*, 6559−6565.
(42) Quinn, B. M.; van 't Ho, P. G.; Lemay, S. G. *J. Am. Chem. Soc.* **2004**, *126*, 8360−8361.
(43) Burt, D. P.; Wilson, N. R.; Weaver, J. M. R.; Dobson, P. S.; Macpherson, J. V. *Nano Lett.* **2005**, *5*, 639−643.
(44) Hafner, J. H.; Cheung, C. L.; Lieber, C. M. *J. Am. Chem. Soc.* **1999**, *121*, 9750−9751.
(45) Wong, S. S.; Joselevich, E.; Woolley, A. T.; Cheung, C. L.; Lieber, C. M. *Nature* **1998**, *394*, 52−55.
(46) Shao, Y. H.; Mirkin, M. V.; Fish, G.; Kokotov, S.; Palanker, D.; Lewis, A. *Anal. Chem.* **1997**, *69*, 1627−1634.
(47) Mezour, M. A.; Morin, M.; Mauzeroll, J. *Anal. Chem.* **2011**, *83*, 2378−2382.
(48) Jena, B. K.; Percival, S. J.; Zhang, B. *Anal. Chem.* **2010**, *82*, 6737−6743.
(49) Li, Y.; Bergman, D.; Zhang, B. *Anal. Chem.* **2009**, *81*, 5496−5502.
(50) Katemann, B. B.; Schuhmann, T. *Electroanalysis* **2002**, *14*, 22−28.
(51) Bard, A. J.; Fan, F. R. F.; Kwak, J.; Lev, O. *Anal. Chem.* **1989**, *61*, 132−138.
(52) Shen, M.; Arroyo-Curras, N.; Bard, A. J. *Anal. Chem.* **2011**, *83*, 9082−9085.
(53) Aoki, K.; Zhang, C. F.; Chen, J. Y.; Nishiumi, T. *Electrochim. Acta* **2010**, *55*, 7328−7333.
(54) Etienne, M.; Moulin, J.-P.; Gourhand, S. *Electrochim. Acta* **2013**, *110*, 16−21.
(55) Liu, B.; Rolland, J. P.; DeSimone, J. M.; Bard, A. J. *Anal. Chem.* **2005**, *77*, 3013−3017.
(56) Potjekamloth, K.; Janata, J.; Josowicz, M. *Berichte Der Bunsen-Gesellschaft-Physical Chem. Chem. Phys.* **1989**, *93*, 1480−1485.
(57) Schulte, A.; Chow, R. H. *Anal. Chem.* **1996**, *68*, 3054−3058.
(58) Penner, R. M.; Heben, M. J.; Lewis, N. S. *Anal. Chem.* **1989**, *61*, 1630−1636.

DOI: 10.1021/acs.analchem.5b03548
Anal. Chem. 2016, 88, 614−620

(59) Morris, C. A.; Friedman, A. K.; Baker, L. A. *Analyst* **2010**, *135*, 2190−2202.
(60) Dickey, M. D.; Chiechi, R. C.; Larsen, R. J.; Weiss, E. A.; Weitz, D. A.; Whitesides, G. M. *Adv. Funct. Mater.* **2008**, *18*, 1097−1104.
(61) Cortes-Salazar, F.; Deng, H.; Peljo, P.; Pereira, C. M.; Kontturi, K.; Girault, H. H. *Electrochim. Acta* **2013**, *110*, 22−29.
(62) Velmurugan, J.; Zhan, D.; Mirkin, M. V. *Nat. Chem.* **2010**, *2*, 498−502.
(63) Everson, M. P.; Helms, J. H. *Synth. Met.* **1991**, *40*, 97−109.
(64) Zoski, C. G.; Mirkin, M. V. *Anal. Chem.* **2002**, *74*, 1986−1992.

DOI: 10.1021/acs.analchem.5b03548
Anal. Chem. 2016, 88, 614−620